

Development of phenothiazine-based theranostic compounds that act both as inhibitors of β -amyloid aggregation and imaging probes for amyloid plaques in Alzheimer's disease

Pascal Dao, Feifei Ye, Yan Liu, Zhiyun Du, Kun Zhang,
Chang-Zhi Dong, Bernard Meunier, and Huixiong CHEN

ACS Chem. Neurosci., **Just Accepted Manuscript** • DOI: 10.1021/acschemneuro.6b00380 • Publication Date (Web): 18 Jan 2017

Downloaded from <http://pubs.acs.org> on January 19, 2017

Just Accepted

"Just Accepted" manuscripts have been peer-reviewed and accepted for publication. They are posted online prior to technical editing, formatting for publication and author proofing. The American Chemical Society provides "Just Accepted" as a free service to the research community to expedite the dissemination of scientific material as soon as possible after acceptance. "Just Accepted" manuscripts appear in full in PDF format accompanied by an HTML abstract. "Just Accepted" manuscripts have been fully peer reviewed, but should not be considered the official version of record. They are accessible to all readers and citable by the Digital Object Identifier (DOI®). "Just Accepted" is an optional service offered to authors. Therefore, the "Just Accepted" Web site may not include all articles that will be published in the journal. After a manuscript is technically edited and formatted, it will be removed from the "Just Accepted" Web site and published as an ASAP article. Note that technical editing may introduce minor changes to the manuscript text and/or graphics which could affect content, and all legal disclaimers and ethical guidelines that apply to the journal pertain. ACS cannot be held responsible for errors or consequences arising from the use of information contained in these "Just Accepted" manuscripts.

1
2
3 **Development of phenothiazine-based theranostic compounds that act both**
4 **as inhibitors of β -amyloid aggregation and imaging probes for amyloid**
5 **plaques in Alzheimer's disease**
6
7
8
9

10 Pascal Dao, † Feifei Ye, † Yan Liu, † Zhi Yun Du, † Kun Zhang, † Chang Zhi Dong, †, † Bernard
11 Meunier, †, ‡ Huixiong Chen. *, †, §

12 † Faculty of Light Industry and Chemical Engineering, Guang Dong University of Technology, Guang Dong,
13 510006, China, § CNRS, UMR8601, Laboratoire de Chimie et Biochimie Pharmacologiques et Toxicologiques,
14 CBNIT, Université Paris Descartes, PRES Sorbonne Paris Cité, UFR Biomédicale, 45 rue des Saints-Pères,
15 75270 Paris Cedex 06, France, † Université Paris Diderot, Sorbonne Paris Cité, ITODYS, UMR 7086 CNRS, 15
16 rue J-A de Baïf, 75205 Paris Cedex 13, France, ‡ Laboratoire de Chimie de Coordination du CNRS, 205 Route
17 de Narbonne, 31077 Toulouse Cedex, France

18
19
20
21 **Abstract:** Early detection of Alzheimer's disease (AD) is imperative in enabling the
22 understanding and clinical treatment of this disorder, as well as in preventing its progression. Imaging
23 agents specifically targeting A β plaques in the brain and the retina may lead to the early diagnosis of
24 AD. Among them, near infrared fluorescent imaging has emerged as an attractive tool to
25 noninvasively identify and monitor diseases during the preclinical and early stages. In the present
26 study, we report the design, synthesis and evaluation of a series of new near-infrared fluorescent
27 probes. Most of these probes displayed maximum emission in PBS (> 650 nm), which falls in the good
28 range for NIRF probes. Among them, **4a1** showed the highest affinity towards to A β aggregates (K_d =
29 7.5 nM) and an excellent targeting ability for A β plaques in slices of brain and retina tissue from
30 double transgenic mice. These compounds are also found to effectively prevent A β fibrils formation
31 and disaggregate preformed A β fibrils, showing a promising potential as theranostic agents for the
32 diagnosis and therapy of AD.
33

34
35
36
37
38
39
40 **Keywords:** Alzheimer's disease, Beta-amyloid, Cytotoxicity, NIRF imaging, Inhibitors,
41 Theranostic agents
42

43
44
45 **INTRODUCTION**
46

47
48 Alzheimer's disease (AD) is an age-related devastating neurodegenerative disorder, which
49 severely impacts on the global economic development and healthcare system. The number of
50 patients increases every year and it is expected to expand to 36 million to 115 million in
51 worldwide around the year of 2050.^{1,2} Despite numerous efforts and exponential growth in
52 investment, nearly all "disease-modifying" treatment for AD has failed to show clinical
53 benefits in individuals with symptomatic AD to date.³ One of the most likely explanations for
54
55
56
57
58
59
60

1
2
3 these failures is that the drugs were administered too late in the course of the AD
4 neuropathological processes.⁴ It is a reasonable assumption that these therapies will be more
5 effective when applied before major brain damage has occurred. Therefore, the development
6 of novel biomarkers sensitive to preclinical or early clinical stages of AD is crucial for this
7 devastating disease.⁵

8
9
10
11 According to the amyloid cascade hypothesis, A β aggregates in the brain play a key role
12 in the cascade of event leading to AD.⁶ Their formation arises from the aggregation of
13 peptides A β 40 and A β 42, which are generated from amyloid peptide precursor (APP) by
14 cleavage with β - and γ -secretases.⁷ Recent evidence indicates that A β plaques are a critical
15 mediator of neuritic pathology.⁸ These extracellular plaques and deposits of A β and
16 intracellular NFT became over the years the pathological hallmark of AD and drug targets.
17 Recently the pathology data support a model of AD in which A β depositions precede clinical
18 symptoms by several years.^{9,10} In the second phase of illness, neurofibrillary tangles develop,
19 neurons die, brain atrophy occurs, and cognition declines. Consequently, in vivo imaging of
20 A β is particularly suitable for identifying individuals at risk and in the early stages of AD.
21 Therefore, several strategies have been developed for the imaging of amyloid, namely,
22 radiolabeled amyloid- β peptide (A β) antibodies and peptide fragments, small molecules for
23 PET and SPECT imaging, and compounds for MRI. To date, [¹¹C]PIB is the most extensively
24 studied PET imaging probe for A β plaques in humans,¹¹ while [18F]AV-45 is the first A β
25 imaging probe approved by the FDA.¹²

26
27
28
29
30
31
32
33
34
35
36
37 Compared with nuclear imaging modalities, NIRF imaging has emerged as an attractive
38 tool for optical imaging. NIR light is particularly suitable to be used for in vivo imaging of
39 molecular processes due to its acceptable depth of penetration, non-invasive operation,
40 minimal interferences from auto-fluorescence of biological matter and minimal photo-damage
41 to biological samples.¹³ Furthermore, the optical imaging modality possesses many
42 advantages, as it enables safe detection without radiation exposure and real-time imaging
43 without a time-consuming data acquisition process and requires readily available instruments
44 at moderate cost. So far, NIR fluorescent probes have been mainly used in the oncology field
45 for imaging tumors, both in vitro and in vivo.^{14,15} Recently, a number of NIR fluorophores
46 have also been developed and employed for AD imaging in vivo, including NIAD,¹⁶
47 CRAND,¹⁷ AOI-987,¹⁸ DANIR,¹⁹ BAP²⁰ and THK-265 (figure 1).²¹ AOI-987 is a charged
48 molecule with a small Stokes shift and moderate affinity (K_d = 220 nM), which implies
49 limited BBB permeability and obscured signal increase upon binding with A β plaques. Ran et
50
51
52
53
54
55
56
57
58
59
60

al. have exploited curcumin derivatives as NIR probes for soluble or insoluble A β species. One of these compounds, CRANAD-2 was reported as a NIR probe for A β plaques with advantages over other candidates such as its ideal binding constant ($K_d = 38.7$ nM) and optimal fluorescent properties (emission maximum at 805 nm). However, most of these probes are unable to satisfy the diverse and stringent requirements for cerebral A β species imaging including good BBB permeability, high selectivity and strong binding affinity towards A β species, low neurotoxicity and good bio-stability. On the other hand, few of NIR probes used as molecular theranostics, which could simultaneously perform imaging of A β species and A β aggregation inhibition have been described. It is difficult to predict the full impact of molecular theranostics in the clinical arena. However, they represent a powerful emerging platform that could optimize the efficacy and safety of therapy, as well as yield information about the entire drug development process.

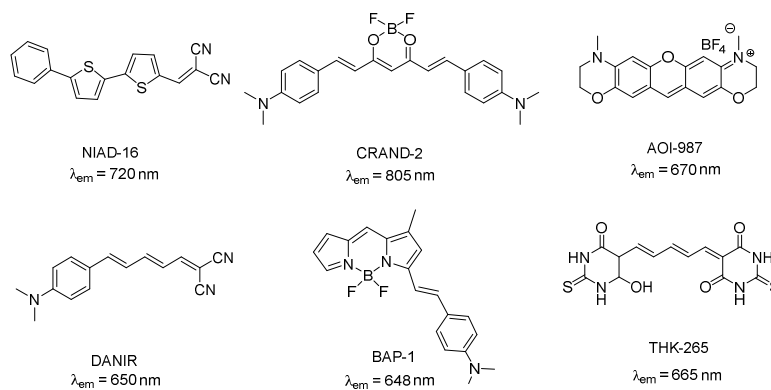
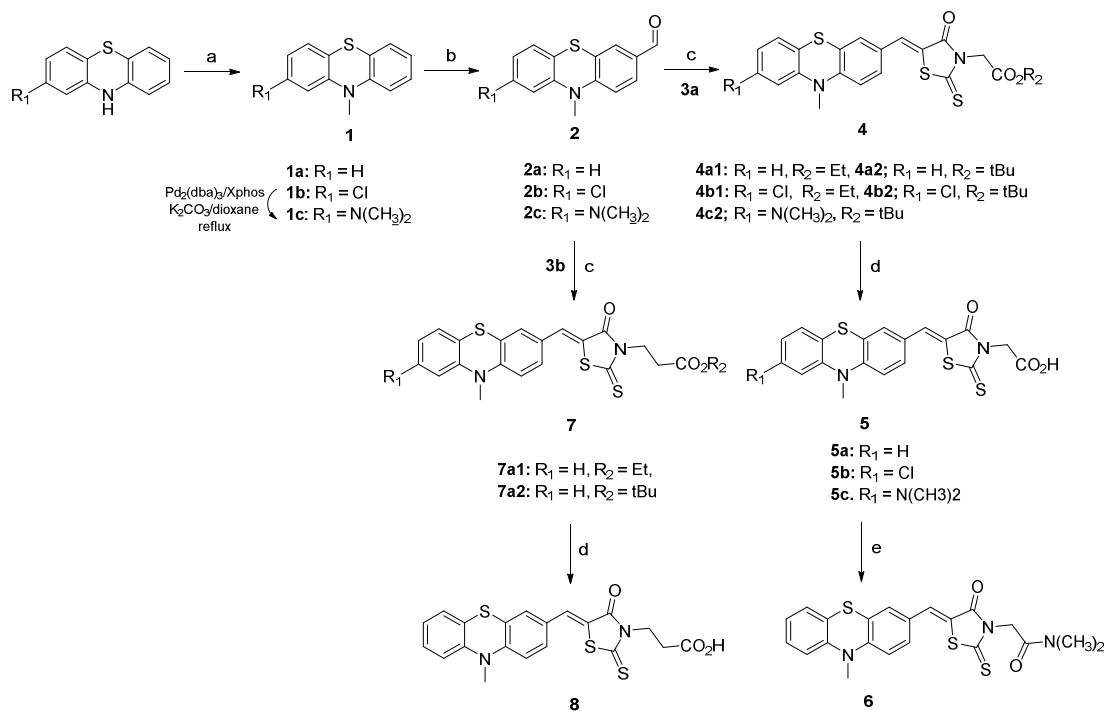


Figure 1. NIRF probes reported previously for the detection of A β plaques.

In an attempt to develop theranostic agents for NIRF imaging of β -amyloid species and inhibition of β -amyloid aggregation, the donor-acceptor architecture bridged by a conjugated π -electron chain was selected as the backbone structure to produce compounds possessing a suitable spectral range of the absorption and emission bands along with a potential to satisfy the necessary requirements for cerebral A β species imaging. Here we report the synthesis, characteristics, and biological evaluations of these theranostic agents as smart NIRF imaging probes for A β plaques with a therapeutic intervention in AD.

RESULTS AND DISCUSSION

The synthetic pathway for the preparation of compounds **4-8** is shown in Scheme 1. The compound **1a-b** was synthesized by reacting phenothiazine with methyl iodide in DMF in the presence of NaH. Nucleophilic displacement of the chloride of **1b** with dimethylamine was performed by Buchwald–Hartwig amination, leading to **1c**. N-methyl phenothiazine derivatives **1a-c** were formylated to their carboxaldehyde derivatives **2a-c** by Vilsmeier formylation procedure by the reaction of the respective compounds with POCl₃ in DMF. The rhodanine core **3** was produced by the reaction of glycine ester or 3-aminopropanoate (ester) with bis(carboxymethyl)trithiocarbonate in the presence of triethylamine. The key step in the formation of the target compounds **4** and **7** were achieved by a Knoevenagel condensation reaction between the phenothiazine-3-carbaldehyde derivatives **2a-c** and the rhodanines **3** in the presence of piperidine. The esters **4a2**, **4b2** and **7a2** can be hydrolyzed to the corresponding carboxylic acids **5**, **8**. Finally, the acid **5a** was converted to the amide **6**, using BOP as a coupling reagent and dimethylamine as a base.

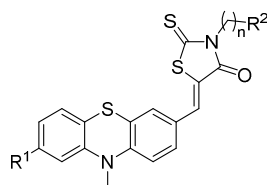


Scheme 1. Conditions and reagents: a) CH₃I, NaH, DMF; b) POCl₃, DMF; c) rhodanine derivatives **3**, piperidine, DCM; d) TFA, DCM; e) BOP, DIPEA.

First, the fluorescent properties, including excitation and emission wavelengths of these compounds in PBS (0.2 M, pH = 7.4) were evaluated. As shown in table 1, except for **5a** and

8, the emission wavelengths for these compounds were ≥ 650 nm, which fall in the good range for NIRF probes. A significant fluorescence intensity increase in the emission of these compounds was observed upon association with A β 1–42 aggregates, especially for the compounds **6**, **5b**, **8** (table 1), which have more than 10-fold intensity increase and suggested that these compounds would be “turned on” upon interacting with a host. However, they did not exhibit the fluorescence enhancement response to A β 1–42 monomer (Figure 2). It suggested that these compounds could binds well to the hydrophobic pockets of A β 1–42 aggregates, resulting in the restricted rotation upon binding to its substrate. This is further reflected by a grand increase in quantum yield upon binding to aggregate β -amyloid proteins, which is a desirable feature for a probe, in order for its fluorescence to be clearly distinguished from that of the background.

Table 1. Molecular weight, fluorescence profile, and fold increase of phenothiazine-based compounds upon interaction with A β 1–42 aggregates



| N ^o | R ₁ | R ₂ | n | λ_{abs} (nm) | λ_{em} (nm) | λ_{em} (nm) with A β | Fold increase | ϵ (M ⁻¹ cm ⁻¹) | Φ (%) |
|----------------|----------------------------------|--|---|--------------------------------|-------------------------------|--|------------------|---|----------------------------|
| 4a1 | H | CO ₂ Et | 1 | 500 | 680 | 670 | 4.89 | 8377.0 | 5.3, 25.1 ^a |
| 4a2 | H | CO ₂ tBu | 1 | 490 | 670 | 670 | 2.48 | 6061.7 | 6.6, 18.0 ^a |
| 4b1 | Cl | CO ₂ Et | 1 | 470 | 660 | 660 | 6.2 | 6888.6 | 10.4, 49.8 ^a |
| 4b2 | Cl | CO ₂ tBu | 1 | 470 | 660 | 660 | 2.9 | 7532.2 | 7.1, 17.8 ^a |
| 4c2 | N(CH ₃) ₂ | CO ₂ tBu | 1 | 510 | 680 | 670 | 2.3 | 8575.7 | 5.0 6.9 ^a |
| 5a | H | CO ₂ H | 1 | 470 | 650 | 640 | 7.3 | 5756.7 | 4.6 16.5 ^a |
| 5b | Cl | CO ₂ H | 1 | 470 | 640 | 640 | 11.1 | 7089.1 | 0.3 1.2 ^a |
| 5c | N(CH ₃) ₂ | CO ₂ H | 1 | 500 | 680 | 670 | 3.2 | 6098.6 | 0.1 0.9 ^a |
| 6 | H | CO ₂ N(CH ₃) ₂ | 1 | 480 | 680 | 680 | 13.1 | 4565.7 | 2.0, 12.1 ^a |
| 7a1 | H | CO ₂ Et | 2 | 490 | 670 | 670 | 6.4 | 6377.0 | 4.3, 57.6 ^a |
| 7a2 | H | CO ₂ tBu | 2 | 480 | 660 | 660 | 3.9 | 5671.8 | 10.1, 66.1 ^a |
| 8 | H | CO ₂ H | 2 | 470 | 640 | 640 | 11.0 | 6061.3 | 0.2 5.9 ^a |

^awith A β 1-42 aggregates

A useful NIRF A β -binding probe should have weak interactions with serum albumin and low cytotoxicity. Firstly, we compared the fluorescent properties of these free probes in aqueous solution to their fluorescence properties in the presence of A β 1–42 aggregates and bovine serum albumin (BSA). As shown in Figure 2, no significant change in fluorescence was observed during incubation with BSA, suggesting that there is little or no interaction between **4a1** (or **5a**) and BSA. Then, a cytotoxicity study of **4a1** was carried out by MTT assays with or without exposure to light using a human neuronal cell line (SH-SY5Y) at different concentrations. As shown in Figure 3, probe **4a1** did not show marked toxicity to this human neuronal cell line at 50 μ M.

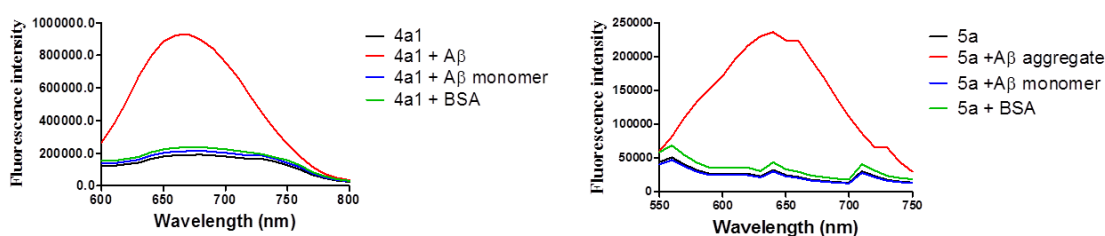


Figure 2. Emission spectra of **4a1** and **5a** (1 μ M) upon interaction with A β aggregates or monomer and BSA.

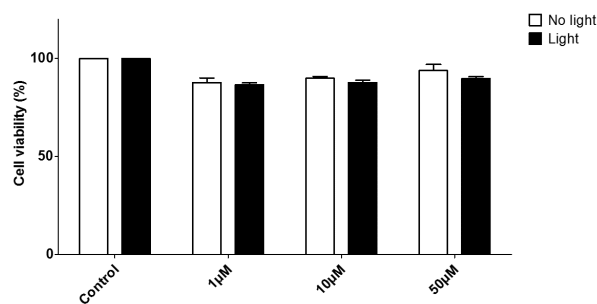
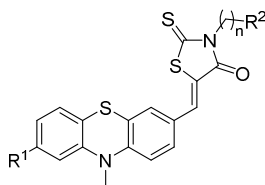


Figure 3. Cell viability after incubation of **4a1** at different concentrations with a human neuronal cell line (SH-SY5Y) by MTT assay, at 37 $^{\circ}$ C for 24 h with or without exposure to light (each sample was tested using three replicates, and the results are reported as the mean \pm standard deviation).

To quantitatively evaluate the binding affinities of these probes to A β 1–42 aggregates, an in vitro saturation binding assay using A β 1–42 aggregates was performed according to conventional methods. In the results shown in table 2, these compounds showed moderate to high affinity to A β 1–42 aggregates, which were significantly higher than that of ThT, widely used for detecting protein and peptide aggregation such as A β aggregation ($K_d = 1.7 \mu$ M). The lipophilicity ($\log P$ with 2–3.5 range) and molecular weight (less than 600 Da) of the probes are two primary factors affecting the capability of BBB penetration. As shown in table

2, several compounds were found to have calculated $\log P$ values between 2.0 and 3.5, suggesting that they can potentially cross the BBB efficiently.

Table 2. Dissociation constant of phenothiazine-based compounds to A β 1–42 aggregates and inhibition of A β 1–42 aggregation

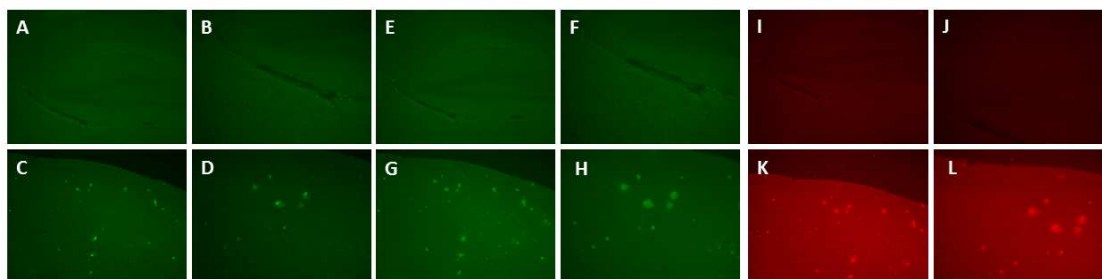


| N ^o | R ₁ | R ₂ | m | M | logP ^a | Kd (nM) | Inhibition of A β aggregation IC ₅₀ (μ M) |
|-----------------|----------------------------------|--|---|-------|-------------------|------------------|---|
| 4a1 | H | CO ₂ Et | 1 | 442.6 | 3.68 | 7.5 \pm 0.4 | 0.67 \pm 0.02 |
| 4a2 | H | CO ₂ tBu | 1 | 470.6 | 4.22 | 41.5 \pm 3.5 | 1.42 \pm 0.06 |
| 4b1 | Cl | CO ₂ Et | 1 | 477.0 | 4.24 | 74.2 \pm 5.4 | 1.52 \pm 0.04 |
| 4b2 | Cl | CO ₂ tBu | 1 | 505.1 | 4.78 | 117.3 \pm 8.7 | 1.63 \pm 0.02 |
| 4c2 | N(CH ₃) ₂ | CO ₂ tBu | 1 | 513.7 | 4.5 | 237.6 \pm 6.2 | 3.77 \pm 0.08 |
| 5a | H | CO ₂ H | 1 | 414.5 | 3.08 | 146.9 \pm 12.6 | 1.07 \pm 0.02 |
| 5b | Cl | CO ₂ H | 1 | 448.9 | 3.64 | 695.8 \pm 14.9 | 1.85 \pm 0.06 |
| 5c | N(CH ₃) ₂ | CO ₂ H | 1 | 457.6 | 3.37 | 204.8 \pm 20.1 | 4.62 \pm 0.20 |
| 6 | H | CO ₂ N(CH ₃) ₂ | 1 | 441.6 | 3.19 | 96.4 \pm 8.3 | 7.32 \pm 0.90 |
| 7a1 | H | CO ₂ Et | 2 | 456.6 | 3.98 | 28.5 \pm 2.5 | 7.29 \pm 1.0 |
| 7a2 | H | CO ₂ tBu | 2 | 484.7 | 4.51 | 14.9 \pm 1.3 | 8.44 \pm 1.1 |
| 8 | H | CO ₂ H | 2 | 428.6 | 3.38 | 212.5 \pm 24.3 | 1.72 \pm 0.2 |
| ThT | | | | | | 1942 \pm 32.1 | ND |
| Curcumin | | | | | | ND | 17.4 \pm 3.4 |

^alogP values were calculated using chemdraw program

To validate the feasibility of our compounds as a NIR imaging probes to A β plaques, the in vitro neuropathological fluorescent staining of A β plaques in slices of brain tissue from a double transgenic (APPwse/PSEN1, 9-month old) mouse overexpressing A β was performed with **4a1**. As shown in Figure 4K and 4L, specific staining of A β plaques was clearly observed in the brain slices of the Tg mouse, which displayed intense and distinct red fluorescence clusters. The presence and distribution of A β was similar to the observation of staining adjacent slices using Thioflavin-T (ThT) (Figure 4G and 4H). These results were consistent with those observed in a 10-month old double transgenic (APPwse/PSEN1), which showed slightly larger plaques in slices of brain (Figure S-1). However, there were no plaques found in the age-matched wild-type control mouse (Figure 4A, 4B and 4I, 4J). *In vitro* staining of A β plaques in slices of brain tissue from a double transgenic (APPwse/PSEN1, 9-month old) mouse was also performed by IHC with the commercially available A β antibody (Figure

1
2
3 4). There is no plaque deposition in the age-matched wild-type control mouse (Figure 4I, 4G),
4 but distinct fluorescence signals were observed in a double transgenic (APP^{wse}/PSEN1, 9-
5 month old) mouse (Figure 4K, 4L). These results clearly demonstrated that **4a1** can
6 effectively bind to and label A β plaque in the brain slice.
7
8
9



10
11
12
13
14
15
16
17
18
19
20
21 **Figure 4.** Fluorescence staining of **4a1** on brain slices of cortex regions of a double Tg mouse (K and
22 L, magnification: 5X). Adjacent slices from Tg mouse were stained with ThT (C and D,
23 magnification: 5X) and with A β antibody ab2454 then secondary antibody with fluorophore Alexa 488
24 (G and H, magnification: 5X). Brain slices from wild-type control mouse was also used in the same
25 conditions with **4a1** (I and J), ThT (A and B) and A β antibody ab2454 then secondary antibody with
26 fluorophore Alexa 488 (E and F).
27
28
29
30
31
32

33 Then, the fluorescent staining of A β plaques in slices of the eye containing retina tissue
34 from the same double transgenic mouse was also performed. The retina can serve as an
35 excellent alternative system for AD research because it can faithfully reflect the changes in
36 the brain and offers unique advantages that can simplify the investigation of AD. Indeed,
37 being a part of the central nervous system (CNS), the retina contains a high density of
38 neuronal cells with a laminar structure outside the brain. Multiple transgenic mouse lines have
39 elicited AD-like pathological hallmarks in the retina as disease progresses.^{22,23} A β plaques
40 were detected in the retina as early as at 2.5 months of age in AD-Tg mice, but not in the
41 brain, suggesting that A β plaques in the retina preceded brain plaques.²² Furthermore, recent
42 advances of imaging technologies for the retina have given the opportunity for the
43 development of a more definitive and non-invasive diagnostic tool for AD pathology.²⁴ As
44 anticipated, retinal A β plaques were absent in the slices of non-Tg (wt) mice, shown in Figure
45 5, whereas they were clearly identified in the slices of eye containing retina of AD-Tg mice
46 (Figure 5J, 5K). The similar results were confirmed using ThT (Figure 5C and 5D) and A β
47 antibody (Figure 5G and 5H).
48
49
50
51
52
53
54
55
56
57
58
59
60

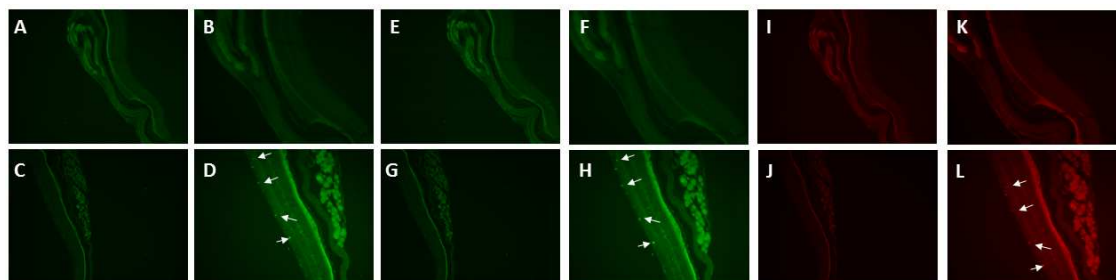


Figure 5. Fluorescence staining of **4a1** on the slices of the eye containing retina tissue of a double Tg mouse (J and L, magnification: 5X). Adjacent slices from Tg mouse were stained with ThT (C and D, magnification: 5X) and with A β antibody ab2454 then secondary antibody with fluorophore Alexa 488 (G and H). Eyes slices from wild-type control mouse was also used in the same conditions with **4a1** (I and K), ThT (A and B) and A β antibody ab2454 then secondary antibody with fluorophore Alexa 488 (E and F).

To explore the potential therapeutic application of our target molecules, we further studied whether these compounds can interfere with A β 1–42 aggregation and its disaggregation. One reported natural product, curcumin which was shown to inhibit the formation of amyloid oligomers and fibrils and to reduce Amyloid *in vivo*,²⁵ was included to validate the screening conditions. Under the experimental conditions, curcumin inhibited A β 1–42 aggregation with IC₅₀ value of 17.4 μ M (Table 2), which was similar to previously reported data. Firstly, the seed-mediated growth of A β 1–42 aggregate was carried out in the presence of compound **4a1** (1 and 10 μ M) or without **4a1**. The resulting aggregates were visualized under the fluorescence microscope. As shown in Figure 6, compound **4a** has significantly slowed down the aggregation rate of A β 1–42 in a dose-dependent manner, as compared with the control. Furthermore, the inhibitory effect of these compounds on the aggregation of A β 1–42 was also investigated. As shown in table 2, all these compounds can effectively inhibit the aggregation of A β 1–42. The IC₅₀ of these compounds was found to be in the range of 0.67–8.44 μ M. Among them, compound **4a1** displayed a strong inhibition on the aggregation of A β 1–42. This results was consistent with the fluorescence microscopy experiments.

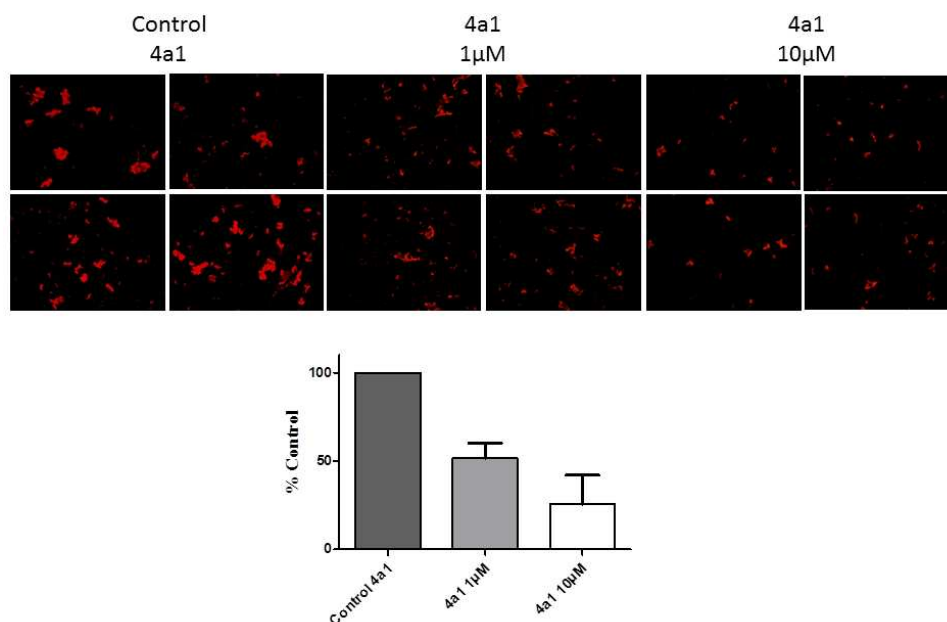


Figure 6. Inhibition of self aggregation of A β 1-42 followed by fluorescence microscopy using **4a1**. Four random fields were presented for each treatment.

Next, we investigated whether these compounds could further disaggregate preformed A β 1-42 fibrils. A β 1-42 fibrils that were generated by 3-days incubation of monomeric A β 1-42 at 37°C were incubated with tested compounds for another 3 days. It was shown that the samples co-incubated with **4a1** or **5a** or curcumin as the standard decreased ThT fluorescence and showed IC₅₀ values of 0.82 ± 0.10 , 1.28 ± 0.35 and 9.9 ± 1.2 μ M, respectively. The target compounds **4a1** and **5a** exhibited markedly higher inhibitory activity than curcumin, suggesting that our target compounds able to promote disassembly preformed A β 1-42 fibrils at low concentrations and are of high potential to be used as therapeutic agents to treat AD. These results were also confirmed by fluorescence microscopy analysis of **4a1** promoting fibril disaggregation (Figure S2). Indeed, the results show that **4a1** has an impact on fibril maturation or dissolution.

CONCLUSION

We successfully designed and synthesized a series of novel smart NIRF probes with donor-acceptor architecture for detection of A β plaques. Most of these probes displayed maximum emission in PBS (≥ 650 nm). Upon binding to A β 1-42 aggregates, these

1
2
3 compounds displayed a significant fluorescence intensity increase in the emission spectra,
4 which is very close to the good range for NIRF imaging. In binding experiments in vitro, they
5 showed good affinity for A β ₁₋₄₂ aggregates. Among them, **4a1** showed the highest affinity
6 (K_d = 7.5 nM). Fluorescence staining of A β plaques in brain and eye slices in vitro
7 demonstrated an excellent targeting ability. From a medicinal chemistry perspective **4a1**
8 offers advantages of a small-molecule scaffold which is easily amenable to further
9 manipulation to improve fluorescence response and amyloid-binding properties. Remarkably,
10 it offers the additional advantage of a concomitant promising profile of A β aggregation
11 inhibition and disaggregation of preformed A β fibrils, together with a high stability in mouse
12 serum and a low toxicity to human neuronal cells. **4a1** will be selected for further studies in
13 the laboratory.
14
15
16
17
18
19
20
21

22 MATERIALS AND METHODS

23
24 All commercial materials were used without further purification. Melting points were
25 determined on a Kofler apparatus as uncorrected values. Analytical thin-layer
26 chromatography was performed on precoated 250 μ m layer thickness silica gel 60 F254 plates
27 and visualized with UV light. Column chromatography was performed using silica gel 60
28 (40–63 μ m). ¹H NMR and ¹³C NMR spectra were measured on 400MHz spectrometer in
29 DMSO-d₆ or CDCl₃ with chemical shift (δ) given in parts per million (ppm) relative to TMS
30 as internal standard and recorded at 23 °C. MS (ESI) was determined by using a QTRAP
31 spectrometer with ion source. The purity of the compounds (>95%) was established by
32 elemental analysis. Fluorescence and ultraviolet–visible spectra were measured using a
33 spectrofluorophotometer (RF-5301PC, Shimadzu, Japan) and a UV spectrophotometer (UV-
34 2450, Shimadzu, Japan), respectively. The fluorescence properties, including absorbance
35 spectrum, excitation and emission wavelengths of the synthesized probes in PBS were
36 evaluated on a multi-mode spectrophotometer (Spectramax Paradigm, Molecular Devices,
37 San Francisco, CA, USA). Fluorescence QYs were measured using an aqueous solution of
38 rhodamine 6G as a standard (Φ = 0.76).
39
40
41
42
43
44
45
46
47
48
49

50 Monomeric A β ₁₋₄₂ was purchased from GL Biochem. Transgenic mice
51 (APP^{Swe}/PSEN1^{dE9}, 9-10 months old, male) and male C57BL/6 counterparts were provided
52 from GDMLAC (certification number: 44007200000555). The animals were sacrificed by
53 decapitation. The brain and eyes of each mouse was removed carefully and cut into slice
54
55
56
57
58
59
60

1
2
3 along the sagittal plane. The protocols of animal test were approved by the Institutional
4 Animal Care and Use Committee of GDMLAC.
5
6

7 **General Method for the Synthesis of compounds 1a and 1b.** A solution of the
8 corresponding compound phenothiazine (10 mmol, 1 equiv) in DMF with CH₃I (20 mmol, 2
9 eq) and NaH (15 mmol, 1.5 equiv) was stirred at RT for 4 h. The solvent was evaporated
10 under vacuum. The crude residue was diluted in ethyl acetate, washed with NaHCO₃, dried
11 over Na₂SO₄, filtered and concentrated. The crude product was purified by silica gel column
12 chromatography eluted with a mixture of petroleum ether and ethyl acetate.
13
14

15 **10-methyl-10H-phenothiazine (1a).** 2.05 g (96%); ¹H NMR (400 MHz, Acetone) δ
16 7.21 (td, *J* = 8.0, 1.5 Hz, 1H), 7.21 (d, *J* = 2.0 Hz, 1H), 7.14 (dd, *J* = 8.0, 1.5 Hz, 2H), 6.96 (d,
17 *J* = 7.0 Hz, 2H), 6.95 (td, *J* = 7.0 Hz, 1.5 Hz, 1H), 3.39 (s, 3H).
18
19

20 **2-chloro-10-methyl-10H-phenothiazine (1b).** 2.40 g (97%); ¹H NMR (400 MHz,
21 CDCl₃) δ 7.16 (td, *J* = 7.8, 1.3 Hz, 1H), 7.12 (dd, *J* = 7.8, 1.3 Hz, 1H), 6.99 (d, *J* = 8.5 Hz,
22 1H), 6.94 (t, *J* = 7.5 Hz, 1H), 6.88 (dd, *J* = 8.5, 2.0 Hz, 1H), 6.78 (d, *J* = 8.5 Hz, 1H), 6.73 (d, *J*
23 = 2.0 Hz, 1H), 3.29 (s, 3H).
24
25
26
27

28 ***N,N*,10-trimethyl-10H-phenothiazin-2-amine (1c).** A solution of **1b** (2 mmol, 1eq) in
29 dioxane with tBuONa (4 mmol, 2eq) was purged with argon before the addition of Pd₂(dba)₃
30 (0.08 mmol, 0.04 eq) and Xphos (0.16 mmol, 0.04 eq). The mixture was stirred at reflux for
31 6h. The mixture was filtered. The solvent was evaporated. Purification by silica gel column
32 chromatography eluted with a mixture of petroleum ether and ethyl acetate provided the title
33 compound as a yellow oil; 328 mg (64%); ¹H NMR (400 MHz, CDCl₃) δ 7.16-7.10 (m, 2H),
34 6.97 (d, *J* = 8.5, 1H), 6.89 (td, *J* = 8.0, 1.0 Hz, 1H), 6.8 (dd, *J* = 8.0, 1.0 Hz, 1H), 6.33 (dd, *J* =
35 8.0, 2.5 Hz, 1H), 6.21 (d, *J* = 2.5, 1H), 3.36 (s, 3 H), 2.92 (s, 6H).
36
37
38
39
40
41

42 **General Method for the Synthesis of compounds 2a-c.** A solution of the
43 corresponding compound (**1a**, **1b** or **1c**, 2.5 mmol, 1 equiv) in DMF was added to a mixture
44 of POCl₃ (7.5 mmol, 3 eq) and DMF (7.5 mmol, 3 eq) at 0°C. The mixture was stirred at RT
45 for 30 min before heating at 100°C for 7h. The mixture was diluted in DCM and washed with
46 brine in three times. The combined organic phase was dried over MgSO₄, filtered and
47 concentrated in vacuum. The crude product was purified by silica gel column chromatography
48 eluted with a mixture of petroleum ether and ethyl acetate.
49
50
51
52

53 **10-methyl-10H-phenothiazine-3-carbaldehyde (2a).** 350 mg (58%); ¹H NMR (400
54 MHz, CDCl₃) δ 9.78 (s, 1H), 7.64 (dd, *J* = 8.7, 2.0 Hz, 1H), 7.59 (d, *J* = 2.0 Hz, 1H), 7.17 (td,
55
56
57
58
59
60

J=7.8, 1.6 Hz, 1H), 7.11 (dd, $J = 7.8$, 1.6 Hz, 1H), 6.97 (t, $J = 7.5$ Hz, 1H), 6.85 (d, $J = 5.4$ Hz, 1H), 6.82 (d, $J = 5.4$ Hz, 1H), 3.41(s, 3H).

8-chloro-10-methyl-10H-phenothiazine-3-carbaldehyde (2b). 262 mg (38%); ^1H NMR (400 MHz, CDCl_3) δ 7.16 (td, $J = 7.8$, 1.4 Hz, 1H), 7.11 (dd, $J = 7.8$, 1.4 Hz, 1H), 7.01 (d, $J = 8.2$ Hz, 1H), 6.93 (td, $J = 7.6$, 0.7 Hz, 1H), 6.88 (dd, $J = 8.2$, 2.0 Hz, 1H), 6.8 (d, $J = 8.2$ Hz, 1H), 6.75 (d, $J = 2.0$ Hz, 1H), 3.35 (s, 3H).

8-(dimethylamino)-10-methyl-10H-phenothiazine-3-carbaldehyde (2c). 305 mg (43%); ^1H NMR (400 MHz, CDCl_3) δ 9.97 (s, 1H), 7.49 (s, 1H), 7.15 (td, $J = 8.0$, 1.5 Hz, 1H), 7.12 (dd, $J = 8.0$, 1.5 Hz, 1H), 6.95 (td, $J = 7.5$, 1.0 Hz, 1H), 6.82 (d, $J = 7.5$ Hz, 1H), 6.32 (s, 1H), 3.42 (s, 3H), 2.91 (s, 6H).

General Method for the Synthesis of compounds 3. A mixture of glycine ethyl ester or tert-butyl ester hydrochloride (3.6 mmol, 1 eq) and bis(carboxymethyl)trithiocarbonate (7.2 mmol, 1.2 eq) in a mixed solvent of 2-propanol (4 mL) and triethylamine (1 mL, 2eq) was stirred for 1 h under reflux. The solvent was removed, and the residue was purified by silica gel chromatography eluted with mixture of petroleum ether and ethyl acetate.

Ethyl 2-(4-oxo-2-thioxothiazolidin-3-yl)acetate (3a1). 639 mg (81%); yellow solid; mp 55°C ; ^1H NMR (400 MHz, CDCl_3) δ 4.65 (s, 2H), 4.19 (q, $J = 7.8$ Hz, 2H), 4.01 (s, 2H), 1.22 (t, $J = 7.8$ Hz, 3H).

tert-butyl 2-(4-oxo-2-thioxothiazolidin-3-yl)acetate (3a2). 605 mg (68%); yellow solid; mp 56°C ; ^1H NMR (400 MHz, CDCl_3) δ 4.62 (s, 2H), 4.07 (s, 2H), 1.46 (s, 9H).

Ethyl 3-(4-oxo-2-thioxothiazolidin-3-yl)propanoate (3b1). 781 mg (93%); yellow solid; mp 53°C ; ^1H NMR (400 MHz, CDCl_3) δ 4.30 (t, $J = 7.8$ Hz, 2H), 4.18 (q, $J = 7.8$ Hz, 2H), 4.00 (s, 2H), 2.68 (t, $J = 7.8$ Hz, 2H), 1.27 (t, $J = 7.7$ Hz, 3H).

tert-butyl 3-(4-oxo-2-thioxothiazolidin-3-yl)propanoate (3b2). 583 mg (62%); yellow solid; mp 52°C ; ^1H NMR (400 MHz, CDCl_3) δ 4.25 (t, $J = 7.8$ Hz, 2H), 3.98 (s, 2H), 2.61 (t, $J = 7.8$ Hz, 2H), 1.45 (s, 9H).

General Method for the Synthesis of compounds 4 and 7. A solution of the corresponding compound (**2a-c**, 0.1 mmol, 1 eq) in DCM with the corresponding N-substituted rhodanines derivatives **3** (0.11 mmol, 1.1 eq) and piperidine (0.2 mmol, 2 eq) was stirred at RT for 10h. The mixture was neutralized with acetic acid, washed with brine, dried over MgSO_4 and concentrated. The crude was purified by silica gel column chromatography eluted with mixture of petroleum ether and ethyl acetate.

(E)-ethyl 2-(5-((10-methyl-10H-phenothiazin-3-yl)methylene)-4-oxo-2-thioxothiazoli

din-3-yl)acetate (4a1). 30 mg (68%); Red solid; mp 162°C; ¹H NMR (400 MHz, CDCl₃) δ 7.62 (s, 1H), 7.3 (dd, *J* = 8.5, 2.0 Hz, 1H), 7.22 (dd, *J* = 2.0 Hz, 1H), 7.17 (td, *J* = 7.6, 1.4 Hz, 1H), 7.12 (dd, *J* = 7.6, 1.2 Hz, 1H), 6.97 (t, *J* = 7.6 Hz, 1H), 6.83 (d, *J* = 8.4 Hz, 1H), 6.82 (d, *J* = 8.2 Hz, 1H), 4.8 (s, 2H), 4.22 (q, *J* = 7.0 Hz, 2H), 3.40 (s, 3H), 1.27 (t, *J* = 7.2 Hz, 3H). ¹³C NMR (400 MHz, CDCl₃) δ 192.71, 167.16, 165.95, 148.18, 144.18, 133.12, 131.14, 128.94, 127.84, 127.47, 127.35, 124.56, 123.55, 122.32, 119.77, 114.70, 114.39, 62.04, 44.91, 30.93, 14.13. MS (ESI) *m/z*: 443.1 [M + H]⁺. Anal. Calcd for C₂₁H₁₈N₂O₃S₃: C, 56.99; H, 4.10; N, 6.33. Found: C, 57.16; H, 4.06; N, 6.26.

(E)-tert-butyl 2-(5-((10-methyl-10H-phenothiazin-3-yl)methylene)-4-oxo-2-thioxothiazolidin-3-yl)acetate (4a2). 37 mg (78%); Red solid; mp 132°C; ¹H NMR (400 MHz, CDCl₃) δ 7.61 (s, 1H), 7.3 (dd, *J* = 8.0, 2.0 Hz, 1H), 7.21 (d, *J* = 2.0 Hz, 1H), 7.17 (td, *J* = 7.5, 1.5 Hz, 1H), 7.12 (dd, *J* = 8.0, 1.5 Hz, 1H), 6.96 (t, *J* = 7.5 Hz, 1H), 6.83 (d, *J* = 8.0 Hz, 1H), 6.82 (d, *J* = 8.0 Hz, 1H), 4.73 (s, 2H), 3.40 (s, 3H), 1.44 (s, 9H). ¹³C NMR (400 MHz, CDCl₃) δ 192.99, 167.40, 165.05, 148.28, 144.38, 133.08, 131.25, 129.10, 127.99, 127.70, 127.51, 124.71, 123.69, 122.51, 120.11, 114.85, 114.54, 83.30, 45.79, 31.10, 20.17. MS (ESI) *m/z*: 471.2 [M + H]⁺. Anal. Calcd for C₂₃H₂₂N₂O₃S₃: C, 58.70; H, 4.71; N, 5.95. Found: C, 58.82; H, 4.65; N, 5.98.

(E)-ethyl 2-(5-((8-chloro-10-methyl-10H-phenothiazin-3-yl)methylene)-4-oxo-2-thioxothiazolidin-3-yl)acetate (4b1). 37 mg (78%); Red solid; mp 173°C; ¹H NMR (400 MHz, CDCl₃) δ 7.61 (s, 1H), 7.31 (dd, *J* = 8.5, 2.0 Hz, 1H), 7.2 (d, *J* = 2.0 Hz, 1H), 7.01 (d, *J* = 8.5 Hz, 1H), 6.94 (dd, *J* = 8.0, 2.0 Hz, 1H), 6.84 (d, *J* = 8.0 Hz, 1H), 6.89 (d, *J* = 2.0 Hz, 1H), 4.83 (s, 2H), 4.22 (q, *J* = 7.0 Hz, 2H), 3.38 (s, 3H), 1.27 (t, *J* = 7.0 Hz, 3H). ¹³C NMR (400 MHz, CDCl₃) δ 191.53, 166.68, 164.90, 146.33, 144.37, 132.78, 131.70, 130.10, 129.88, 127.83, 126.76, 123.29, 122.23, 119.78, 119.32, 114.08, 113.66, 61.03, 43.88, 34.72, 13.15. MS (ESI) *m/z*: 477.2 [M + H]⁺. Anal. Calcd for C₂₁H₁₇ClN₂O₃S₃: C, 52.88; H, 3.59; N, 5.87. Found: C, 52.72; H, 3.63; N, 5.90.

(E)-tert-butyl 2-(5-((8-chloro-10-methyl-10H-phenothiazin-3-yl)methylene)-4-oxo-2-thioxothiazolidin-3-yl)acetate (4b2). 41 mg (83%); Red solid; mp 208°C; ¹H NMR (400 MHz, CDCl₃) δ 7.60 (s, 1H), 7.3 (dd, *J* = 8.5, 2.0 Hz, 1H), 7.2 (d, *J* = 2.0 Hz, 1H), 7.02 (d, *J* = 8.0 Hz, 1H), 6.94 (dd, *J* = 8.5, 2.0 Hz, 1H), 6.84 (d, *J* = 8.0 Hz, 1H), 6.79 (d, *J* = 2.0 Hz, 1H), 4.73 (s, 2H), 3.38 (s, 3H), 1.23 (s, 9H). ¹³C NMR (400 MHz, CDCl₃) δ 192.68, 167.16, 164.83, 147.30, 145.43, 132.52, 132.35, 130.90, 128.86, 128.01, 127.82, 124.32, 123.24, 120.84, 120.52, 115.10, 114.68, 83.15, 45.62, 35.73, 28.00. MS (ESI) *m/z*: 505.1 [M + H]⁺.

Anal. Calcd for C₂₃H₂₁ClN₂O₃S₃: C, 54.70; H, 4.19; N, 5.55. Found: C, 54.84; H, 4.13; N, 5.49.

(E)-tert-butyl 2-(5-((8-(dimethylamino)-10-methyl-10H-phenothiazin-3-yl)methylene)-4-oxo-2-thioxothiazolidin-3-yl)acetate (4c2). 35 mg (69%); Red solid; mp 155°C; ¹H NMR (400 MHz, CDCl₃) δ 7.77 (s, 1H), 7.15 (t, *J* = 8.0 Hz, 1H), 7.13-7.09 (m, 2H), 6.94 (t, *J* = 7.5 Hz, 1H), 6.82 (d, *J* = 8.0 Hz, 1H), 6.45 (s, 1H), 4.72 (s, 2H), 3.40 (s, 3H), 2.71 (s, 6H), 1.44 (s, 9H). ¹³C NMR (400 MHz, CDCl₃) δ 195.24, 167.95, 165.13, 154.54, 149.55, 144.32, 132.42, 129.97, 127.56, 127.32, 123.35, 123.10, 120.45, 119.33, 116.61, 114.65, 104.71, 82.93, 45.64, 44.40, 35.67, 20.01. MS (ESI) *m/z*: 514.2 [M + H]⁺. Anal. Calcd for C₂₅H₂₇N₃O₃S₃: C, 58.45; H, 5.30; N, 8.18. Found: C, 58.62; H, 5.26; N, 8.21.

(E)-ethyl 3-(5-((10-methyl-10H-phenothiazin-3-yl)methylene)-4-oxo-2-thioxothiazolidin-3-yl)propanoate (7a1). 40 mg (87%); Red solid; mp 177°C; ¹H NMR (400 MHz, CDCl₃) δ 7.58 (s, 1H), 7.28 (dd, *J* = 8.5, 2.0 Hz, 1H), 7.2 (d, *J* = 2 Hz, 1H), 7.17 (td, *J* = 7.5, 1.5 Hz, 1H), 7.12 (dd, *J* = 7.5, 1.5 Hz, 1H), 6.96 (t, *J* = 7.5 Hz, 1H), 6.84-6.80 (m, 2H), 4.4 (t, *J* = 7 Hz, 1H), 4.13 (q, *J* = 7 Hz, 1H), 3.40 (s, 3H), 2.73-4 (t, *J* = 7.5 Hz, 2H), 1.54 (s, 4H), 1.24 (t, *J* = 7.5 Hz, 3H). ¹³C NMR (400 MHz, CDCl₃) δ 192.86, 170.62, 167.63, 148.19, 144.33, 132.72, 131.22, 129.04, 127.98, 127.48, 124.67, 123.67, 122.46, 120.02, 114.82, 114.50, 61.11, 40.18, 31.62, 31.07, 14.30. MS (ESI) *m/z*: 457.1 [M + H]⁺. Anal. Calcd for C₂₂H₂₀N₂O₃S₃: C, 57.87; H, 4.42; N, 6.14. Found: C, 57.62; H, 4.50; N, 6.21.

(E)-tert-butyl 3-(5-((10-methyl-10H-phenothiazin-3-yl)methylene)-4-oxo-2-thioxothiazolidin-3-yl)propanoate (7a2). 39 mg (80%); Red solid; mp 182°C; ¹H NMR (400 MHz, CDCl₃) δ 7.57 (s, 1H), 7.29 (dd, *J* = 8.5, 2.0 Hz, 1H), 7.2 (d, *J* = 2 Hz, 1H), 7.17 (td, *J* = 7.5, 1.5 Hz, 1H), 7.12 (dd, *J* = 7.5, 1.5 Hz, 1H), 6.97 (t, *J* = 7.5 Hz, 1H), 6.84-6.80 (m, 2H), 4.36 (t, *J* = 7 Hz, 2H), 3.39 (s, 3H), 2.65 (t, *J* = 7.5 Hz, 2H), 1.42 (s, 9H). ¹³C NMR (400 MHz, CDCl₃) δ 192.73, 170.47, 167.51, 148.07, 144.20, 132.57, 131.06, 128.90, 127.56, 127.35, 124.57, 123.52, 122.34, 119.92, 114.66, 114.34, 60.96, 40.03, 35.65, 31.47, 14.13. MS (ESI) *m/z*: 485.2 [M + H]⁺. Anal. Calcd for C₂₄H₂₄N₂O₃S₃: C, 59.48; H, 4.99; N, 5.78. Found: C, 59.72; H, 4.86; N, 5.61.

General Method for the Synthesis of compounds 5 and 8. A solution of the corresponding compound (**4** or **7**, 0.05 mmol, 1 equiv) was stirred at RT in a mixture of DCM/TFA at a ratio of 2:1 for 4 h. The solvent was concentrated under vacuum before the addition of diethyl ether, the solid was filtrate and wash with diethyl ether.

(E)-2-(5-((10-methyl-10H-phenothiazin-3-yl)methylene)-4-oxo-2-thioxothiazolidin-3-yl)acetic acid (5a). 19 mg (92%); Red solid; mp 253°C; ¹H NMR (400 MHz, Acetone) δ 7.71

(s, 1H), 7.52 (dd, $J = 8.5, 2$ Hz, 1H), 7.4 (d, $J = 2$ Hz, 1H), 7.25 (td, $J = 7.5, 1$ Hz, 1H), 7.17 (dd, $J = 7.5, 1$ Hz, 1H), 7.13 (d, $J = 8.5$ Hz, 1H), 7.05-7.00 (m, 2H), 4.87 (s, 2H), 3.48 (s, 3H). ^{13}C NMR (400 MHz, DMSO) δ 192.68, 167.23, 166.25, 147.67, 143.71, 133.14, 130.97, 129.08, 128.05, 126.98, 126.90, 123.43, 122.86, 120.98, 118.67, 115.30, 115.18, 44.96, 30.63. MS (ESI) m/z : 415.1 $[\text{M} + \text{H}]^+$. Anal. Calcd for $\text{C}_{19}\text{H}_{14}\text{N}_2\text{O}_3\text{S}_3$: C, 55.05; H, 3.40; N, 6.76. Found: C, 54.87; H, 3.49; N, 6.61.

(E)-2-(5-((8-chloro-10-methyl-10H-phenothiazin-3-yl)methylene)-4-oxo-2-thioxothiazolidin-3-yl)acetic acid (5b). 20 mg (91%); Red solid; mp 242°C; ^1H NMR (400 MHz, CDCl_3) δ 7.79 (s, 1H), 7.53 (dd, $J = 8.5, 2.0$ Hz, 1H), 7.46 (d, $J = 2.0$ Hz, 1H), 7.20 (d, $J = 8.0$ Hz, 1H), 7.13 (d, $J = 8.0$ Hz, 1H), 7.09-7.05 (m, 2H), 4.71 (s, 2H), 3.38 (s, 3H). ^{13}C NMR (400 MHz, CDCl_3) δ 189.19, 150.45, 149.89, 144.33, 131.35, 130.00, 129.88, 128.98, 127.84, 126.92, 126.66, 124.26, 112.76, 107.07, 99.43, 39.81, 28.70. MS (ESI) m/z : 449.1 $[\text{M} + \text{H}]^+$. Anal. Calcd for $\text{C}_{19}\text{H}_{13}\text{ClN}_2\text{O}_3\text{S}_3$: C, 50.83; H, 2.92; N, 6.24. Found: C, 50.99; H, 2.86; N, 6.32.

(E)-2-(5-((8-(dimethylamino)-10-methyl-10H-phenothiazin-3-yl)methylene)-4-oxo-2-thioxothiazolidin-3-yl)acetic acid (5c). 21 mg (93%); Red solid; mp 289°C; ^1H NMR (400 MHz, DMSO) δ 7.58 (s, 1H), 7.31 (s, 1H), 7.24 (td, $J = 8.0, 1.5$ Hz, 1H), 7.17 (dd, $J = 8.0, 1$ Hz, 1H), 7.02 (d, $J = 8.0$ Hz, 1H), 7.0 (d, $J = 8.0$ Hz, 1H), 6.67 (s, 1H), 4.70 (s, 2H), 3.41 (s, 3H), 2.70 (s, 6H). ^{13}C NMR (400 MHz, DMSO) δ 195.56, 167.94, 167.63, 154.52, 149.70, 144.37, 133.09, 130.76, 128.34, 127.33, 123.77, 122.21, 119.98, 118.50, 115.81, 115.55, 106.05, 45.46, 44.26, 31.16. MS (ESI) m/z : 458.1 $[\text{M} + \text{H}]^+$. Anal. Calcd for $\text{C}_{21}\text{H}_{19}\text{N}_3\text{O}_3\text{S}_3$: C, 55.12; H, 4.19; N, 9.18. Found: C, 55.72; H, 4.12; N, 9.21.

(E)-3-(5-((10-methyl-10H-phenothiazin-3-yl)methylene)-4-oxo-2-thioxothiazolidin-3-yl)propanoic acid (8). 19 mg (89%); Red solid; mp 250°C; ^1H NMR (400 MHz, DMSO) δ 12.51 (bs, 1H), 7.72 (s, 1H), 7.48 (dd, $J = 8.5, 2.0$ Hz, 1H), 7.42 (d, $J = 2$ Hz, 1H), 7.25 (td, $J = 7.5, 1.5$ Hz, 1H), 7.19 (dd, $J = 7.5, 1.5$ Hz, 1H), 7.11 (d, $J = 8.5$ Hz, 1H), 7.05-6.99 (m, 2H), 4.22 (t, $J = 7$ Hz, 2H), 3.38 (s, 3H), 2.62 (t, $J = 7.5$ Hz, 2H). ^{13}C NMR (400 MHz, CDCl_3) δ 169.68, 166.71, 147.58, 144.59, 143.71, 133.23, 129.92, 128.10, 127.70, 127.27, 125.84, 124.14, 123.18, 123.07, 122.46, 121.08, 114.46, 114.17, 81.25, 40.12, 35.61, 32.54, 28.04. MS (ESI) m/z : 429.1 $[\text{M} + \text{H}]^+$. Anal. Calcd for $\text{C}_{20}\text{H}_{16}\text{N}_2\text{O}_3\text{S}_3$: C, 56.06; H, 3.76; N, 6.54. Found: C, 55.87; H, 3.86; N, 6.45.

(E)-N,N-dimethyl-2-(5-((10-methyl-10H-phenothiazin-3-yl)methylene)-4-oxo-2-thioxothiazolidin-3-yl)acetamide (6). A solution of **4c** (0.05 mmol, 1 eq) in DCM and Dimethylamine (0.1 mmol, 2 eq) and DIPEA (0.13 mmol, 2.5 eq) was added BOP (0.1 mmol,

2 eq). The mixture was stirred for 3h. The mixture was washed with brines, dried over MgSO_4 and concentrated under vacuum. Purified by silica gel column chromatography eluted with a mixture of petroleum ether and ethyl acetate afforded the title compound as a red solid, 20 mg (90 %); mp 217°C; ^1H NMR (400 MHz, CDCl_3) δ 7.61 (s, 1H), 7.3 (dd, $J = 8.5, 2$ Hz, 1H), 7.21 (d, $J = 2$ Hz, 1H), 7.17 (td, $J = 7.5, 1.5$ Hz, 1H), 7.12 (dd, $J = 7.5, 1.5$ Hz, 1H), 6.96 (td, $J = 7.5, 1$ Hz, 1H), 6.85-6.80 (m, 2H), 4.91 (s, 2H), 3.40 (s, 3H), 3.11 (s, 3H), 2.97 (s, 3H). ^{13}C NMR (400 MHz, CDCl_3) δ 192.15, 166.42, 164.90, 147.60, 144.59, 143.92, 133.69, 129.89, 128.14, 127.70, 127.27, 125.89, 124.13, 123.17, 121.03, 114.46, 114.17, 45.57, 35.61, 27.98. MS (ESI) m/z : 442.1 $[\text{M} + \text{H}]^+$. Anal. Calcd for $\text{C}_{21}\text{H}_{19}\text{N}_3\text{O}_2\text{S}_3$: C, 57.12; H, 4.34; N, 9.52. Found: C, 57.47; H, 4.45; N, 9.57.

Preparation of $\text{A}\beta$ monomer and aggregates. $\text{A}\beta_{1-42}$ monomer was prepared by dissolving $\text{A}\beta_{1-42}$ powder in HFIP,¹¹ which is sonicated and stirred for 24h at RT before dried under argon to give a clear film. $\text{A}\beta_{1-42}$ monomer was re-suspended in DMSO (200 μM), and stored at -20°C prior to use. $\text{A}\beta_{1-42}$ aggregates were prepared using the solution of $\text{A}\beta_{1-42}$ monomer (200 μM in DMSO), which was diluted with PBS buffer (pH 7.4) at 20 μM , stirred at 37°C for 2 days, and store at -20°C.

Tissue Preparation. Brain and eyes were collected from each mouse, formalin-fixed and embedded in paraffin. Then, the brain was coronally sectioned (4 μm) and the eyes was sagittally sectioned (4 μm).

Fluorescence studies upon binding to $\text{A}\beta_{1-42}$ aggregates and BSA. A solution of 10 μL of aggregated $\text{A}\beta_{1-42}$ (2 μM) or BSA (40 $\mu\text{g/mL}$) was added to the fluorescent probes (10 μL , 1 μM in PBS, pH 7.4) in a final volume of 20 μL . The mixture was incubated for 30 min at RT, and the fluorescent parameters (fluorescence excitation/emission wavelength and intensity) were measured by a multi-mode spectrophotometer (Spectramax Paradigm, Molecular Devices, San Francisco, CA, USA).

Measurement of cell viability. Cell viability was determined by a quantitative colorimetric assay using MTT. SH-SY5Y cells were seeded at 5000 cells per well in 96-well plates and incubated overnight. Then the cells were treated with the compounds at different concentrations for 1h before exposed to a laser of an spectrum imaging system or not. After further incubation for 48 h, MTT solution (2 mg/mL) was added, and the cells were incubated for another 30 min. The absorbance of each well was measured at 570 nm.

1
2
3 ***In vitro* A β ₁₋₄₂ aggregates binding constant measurement.** A solution of aggregated
4 A β ₁₋₄₂ aggregates (1 μ M in the final assay mixture) was mixed with different concentrations
5 of the fluorescent probes (10^{-5} to 10^{-10} in PBS) and incubated for 30 min at RT. The
6 fluorescent intensity was measured by a multi-mode spectrophotometer (Spectramax
7 Paradigm, Molecular Devices, San Francisco, CA, USA). The resulting intensities, corrected
8 where for background fluorescence were plotted in Grafpad Prism. Kd values were
9 determined using the single-site ligand binding module. Each measurement was run in
10 triplicate.
11
12
13
14
15

16
17 ***In vitro* staining of A β plaques in transgenic mouse brain and eye.** Paraffin-
18 embedded brain and eye tissue from double transgenic mouse and control mouse were used
19 for in vitro fluorescent staining. The brain (4 μ m) and eye (4 μ m) sections were deparaffinized
20 with 2x20 min washes in xylene, 2x5 min washes in 80% ethanol/H₂O, a 5 min wash in 60%
21 ethanol/H₂O and running tap water for 10 min and then incubated in PBS for 30 min.
22
23
24
25

26 For fluorescent staining of A β plaques, they were incubated with fluorescent probe **4a1**
27 (10 nM) for 30 min. The location of plaques was confirmed by staining adjacent section with
28 ThT. Finally, the sections were washed with 40% ethanol and PBS for 10 min.
29
30
31

32 For *in vitro* staining of A β plaques with A β antibody, they were incubated with primary
33 A β antibody (ab2454, Cell signaling, dilution ratio A: 500) at 4°C overnight. The sections
34 were washed with 3x5 min PBS and incubated with secondary antibody with fluorophore
35 Alexa 488 (Invitrogen, dilution ratio 1:200) for 60 min and then washed with 3x5 min PBS.
36
37
38

39 Fluorescent observation was performed using a fluorescence microscope (Olympus
40 IX71 inverted fluorescence microscope).
41
42

43 ***In vitro* inhibition and disaggregation of A β 1-42 Aggregation.** Inhibition of A β 1-42
44 aggregation was performed by incubation of a mixture of A β 1-42 monomer (10 μ L, 20 μ M)
45 with or without the tested compound (10 μ L, 2 μ M) at 37°C for 48 h. 20 μ L of thioflavin-T at
46 5 μ M was added. The fluorescence intensities were recorded 5 min later (excitation 450 nm;
47 emission 485 nm). The percent inhibition of aggregation was calculated by the expression (1-
48 IFi/IFc)*100, in which IFi and IFc are the fluorescence intensities obtained for A β in the
49
50
51
52
53
54
55
56
57
58
59
60

1
2
3 presence and absence of inhibitors after subtracting the background, respectively. Each
4
5 measurement was run in triplicate.
6
7

8 Disaggregation of preformed A β aggregates was carried out as following: A β 1-42
9
10 monomer (20 μ M) was incubated for 3 days at 37°C to generate aggregates. Then the solution
11
12 was mixed with or without the tested compound at various concentrations and incubated for 3
13
14 days at 37°C. Finally, ThT at 5 μ M was added and the fluorescence intensities were recorded
15
16 (excitation 440 nm, emission 480 nm).
17
18
19

20 **Fluorescence staining of inhibition of self-aggregation.** The inhibition of A β 1-42
21
22 self-aggregation was followed by fluorescence microscopy. A β 1-42 monomer (50 μ L, 20 μ M)
23
24 with or without the tested compound (50 μ L, 2 μ M or 20 μ M) at 37°C for 48 h. The formation
25
26 of aggregate was observed by fluorescence microscope (Olympus IX71 inverted fluorescence
27
28 microscope). Digital images of four random fields were taken at 10x magnification. The
29
30 fluorescence intensity was calculated by measuring the average pixel intensity per field with
31
32 the program ImageJ.
33
34
35

36 **Statistical Analysis.** Data were analyzed using the InStat software program (GraphPad
37
38 Software, San Diego, CA). Student's t test was used. All values are expressed as mean \pm SD.
39
40 $p \leq 0.05$ was considered statistically significant.
41
42
43
44

45 **AUTHOR INFORMATION**

46
47 Corresponding Author

48
49 *Permanent address: CNRS, UMR8601, Laboratoire de Chimie et Biochimie
50
51 Pharmacologiques et Toxicologiques, CBNIT, Université Paris Descartes, PRES Sorbonne
52
53 Paris Cité, UFR Biomédicale, 45 rue des Saints-Pères, 75270 Paris Cedex 06, France. E-mail:
54
55 huixiong.chen@parisdescartes.fr. Phone: 33-1-42864085, Fax: 33-1-42864082.
56
57
58
59
60

Author contributions

HC and PD conceived and designed the experiments. PD and FY performed the experiments. HC, PD, ZYD, KZ, CZD and BM analyzed the data. YL contributed reagents, materials, and analysis tools. HC and PD wrote the paper.

Funding

This study is supported by China Postdoctoral Science Foundation (grant no.2015M572280) and China Science Foundation (grant no. 21672043).

Notes

The authors declare no competing financial interest.

ACKNOWLEDGEMENTS

The technical assistance of Guo Q. H. and Wang G. H. is gratefully acknowledged.

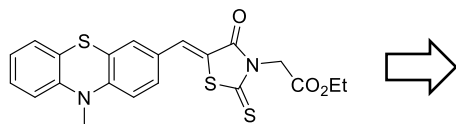
REFERENCE

1. Thies W, Bleiler L. (2016) 2016 Alzheimer's disease facts and figures. *Alzheimers Dement. J. Alzheimers Assoc.* 12, 459–509.
2. Shatenstein, B., Barberger-Gateau, P., and Mecocci, P. (2015) Prevention of Age-Related Cognitive Decline: Which Strategies, When, and for Whom? *J. Alzheimers Dis. JAD48*, 35–53.
3. Lang, A. E. (2010) Clinical trials of disease-modifying therapies for neurodegenerative diseases: the challenges and the future. *Nat. Med.* 16, 1223–1226.
4. Salloway, S., Sperling, R., and Brashear, H. R. (2014) Phase 3 trials of solanezumab and bapineuzumab for Alzheimer's disease. *N. Engl. J. Med.* 370, 1460.
5. Jack, C. R., Albert, M. S., Knopman, D. S., McKhann, G. M., Sperling, R. A., Carrillo, M. C., Thies, B., and Phelps, C. H. (2011) Introduction to the recommendations from the National Institute on Aging-Alzheimer's Association workgroups on diagnostic guidelines for Alzheimer's disease. *Alzheimers Dement. J. Alzheimers Assoc.* 7, 257–262.
6. Hardy, J., and Selkoe, D. J. (2002) The amyloid hypothesis of Alzheimer's disease: progress and problems on the road to therapeutics. *Science* 297, 353–356.

- 1
2
3 7. Selkoe, D. J. (1999) Translating cell biology into therapeutic advances in Alzheimer's
4 disease. *Nature* 399, A23-31.
5
6 8. Meyer-Luehmann, M., Spires-Jones, T. L., Prada, C., Garcia-Alloza, M., de Calignon, A.,
7 Rozkalne, A., Koenigsknecht-Talboo, J., Holtzman, D. M., Bacskai, B. J., and Hyman, B. T.
8 (2008) Rapid appearance and local toxicity of amyloid-beta plaques in a mouse model of
9 Alzheimer's disease. *Nature* 451, 720–724.
10
11 9. Bolognesi, M. L. (2013) Amyloid Chemical Probes and Theranostics: Steps Toward
12 Personalized Medicine in Neurodegenerative Diseases, in *Medicinal Chemistry Approaches to*
13 *Personalized Medicine* (Lackey, K., and Roth, B. D., Eds.), pp 211–226. Wiley-VCH Verlag
14 GmbH & Co. KGaA.
15
16 10. Staderini, M., Martín, M. A., Bolognesi, M. L., and Menéndez, J. C. (2015) Imaging of β -
17 amyloid plaques by near infrared fluorescent tracers: a new frontier for chemical
18 neuroscience. *Chem. Soc. Rev.* 44, 1807–1819.
19
20 11. Kadir, A., Marutle, A., Gonzalez, D., Schöll, M., Almkvist, O., Mousavi, M., Mustafiz,
21 T., Darreh-Shori, T., Nennesmo, I., and Nordberg, A. (2011) Positron emission tomography
22 imaging and clinical progression in relation to molecular pathology in the first Pittsburgh
23 Compound B positron emission tomography patient with Alzheimer's disease. *Brain J.*
24 *Neurol.* 134, 301–317.
25
26 12. Camus, V., Payoux, P., Barré, L., Desgranges, B., Voisin, T., Tauber, C., La Joie, R.,
27 Tafani, M., Hommet, C., Chételat, G., Mondon, K., de La Sayette, V., Cottier, J. P., Beaufils,
28 E., Ribeiro, M. J., Gissot, V., Vierron, E., Vercoillie, J., Vellas, B., Eustache, F., and
29 Guilloteau, D. (2012) Using PET with 18F-AV-45 (florbetapir) to quantify brain amyloid load
30 in a clinical environment. *Eur. J. Nucl. Med. Mol. Imaging* 39, 621–631.
31
32 13. Raymond, S. B., Kumar, A. T. N., Boas, D. A., and Bacskai, B. J. (2009) Optimal
33 parameters for near infrared fluorescence imaging of amyloid plaques in Alzheimer's disease
34 mouse models. *Phys. Med. Biol.* 54, 6201.
35
36 14. Yi, X., Wang, F., Qin, W., Yang, X., and Yuan, J. (2014) Near-infrared fluorescent probes
37 in cancer imaging and therapy: an emerging field. *Int. J. Nanomedicine* 9, 1347–1365.
38
39 15. Kosaka, N., Ogawa, M., Choyke, P. L., and Kobayashi, H. (2009) Clinical implications of
40 near-infrared fluorescence imaging in cancer. *Future Oncol. Lond. Engl.* 5, 1501–1511.
41
42 16. Nesterov, E. E., Skoch, J., Hyman, B. T., Klunk, W. E., Bacskai, B. J., and Swager, T. M.
43 (2005) In Vivo Optical Imaging of Amyloid Aggregates in Brain: Design of Fluorescent
44 Markers. *Angew. Chem. Int. Ed.* 44, 5452–5456.
45
46
47
48
49
50
51
52
53
54
55
56
57
58
59
60

- 1
2
3 17. Ran, C., Xu, X., Raymond, S. B., Ferrara, B. J., Neal, K., Bacskai, B. J., Medarova, Z.,
4 and Moore, A. (2009) Design, synthesis, and testing of difluoroboron-derivatized curcumins
5 as near-infrared probes for in vivo detection of amyloid-beta deposits. *J. Am. Chem. Soc.* *131*,
6 15257–15261.
7
8
9 18. Hintersteiner, M., Enz, A., Frey, P., Jatton, A.-L., Kinzy, W., Kneuer, R., Neumann, U.,
10 Rudin, M., Staufienbiel, M., Stoeckli, M., Wiederhold, K.-H., and Gremlich, H.-U. (2005) In
11 vivo detection of amyloid-beta deposits by near-infrared imaging using an oxazine-derivative
12 probe. *Nat. Biotechnol.* *23*, 577–583.
13
14 19. Fu, H., Tu, P., Zhao, L., Dai, J., Liu, B., and Cui, M. (2016) Amyloid- β Deposits Target
15 Efficient Near-Infrared Fluorescent Probes: Synthesis, in Vitro Evaluation, and in Vivo
16 Imaging. *Anal. Chem.* *88*, 1944–1950.
17
18 20. Ono, M., Watanabe, H., Kimura, H., and Saji, H. (2012) BODIPY-based molecular probe
19 for imaging of cerebral β -amyloid plaques. *ACS Chem. Neurosci.* *3*, 319–324.
20
21 21. Okamura, N., Mori, M., Furumoto, S., Yoshikawa, T., Harada, R., Ito, S., Fujikawa, Y.,
22 Arai, H., Yanai, K., and Kudo, Y. (2011) In vivo detection of amyloid plaques in the mouse
23 brain using the near-infrared fluorescence probe THK-265. *J. Alzheimers Dis. JAD23*, 37–48.
24
25 22. Koronyo-Hamaoui, M., Koronyo, Y., Ljubimov, A. V., Miller, C. A., Ko, M. K., Black,
26 K. L., Schwartz, M., and Farkas, D. L. (2011) Identification of amyloid plaques in retinas
27 from Alzheimer's patients and noninvasive in vivo optical imaging of retinal plaques in a
28 mouse model. *NeuroImage 54 Suppl 1*, S204-217.
29
30 23. Frost, S., Kanagasingam, Y., Sohrabi, H., Vignarajan, J., Bourgeat, P., Salvado, O.,
31 Villemagne, V., Rowe, C. C., Macaulay, S. L., Szoeke, C., Ellis, K. A., Ames, D., Masters, C.
32 L., Rainey-Smith, S., Martins, R. N., and AIBL Research Group, null. (2013) Retinal
33 vascular biomarkers for early detection and monitoring of Alzheimer's disease. *Transl.*
34 *Psychiatry* *3*, e233.
35
36 24. Cordeiro, M. F., Guo, L., Coxon, K. M., Duggan, J., Nizari, S., Normando, E. M., Sensi,
37 S. L., Sillito, A. M., Fitzke, F. W., Salt, T. E., and Moss, S. E. (2010) Imaging multiple phases
38 of neurodegeneration: a novel approach to assessing cell death in vivo. *Cell Death Dis.* *1*, e3.
39
40 25. Yang F., Lim G. P., Begum A. N., Ubeda O. J., Simmons M. R., Ambegaokar S. S., Chen
41 P. P., Kaye R., Glabe C. G., Frautschy S. A., Cole G. M. (2005) Curcumin inhibits formation
42 of amyloid beta oligomers and fibrils, binds plaques, and reduces amyloid in vivo. *J. Biol.*
43 *Chem.* *280(7)*:5892-901.
44
45
46
47
48
49
50
51
52
53
54
55
56
57
58
59
60

1
2
3
4
5
6
7
8
9
10
11
12
13
14
15
16
17
18
19
20
21
22
23
24
25
26
27
28
29
30
31
32
33
34
35
36
37
38
39
40
41
42
43
44
45
46
47
48
49
50
51
52
53
54
55
56
57
58
59
60



4a

λ_{em} : 670 nm

Kd : 7.5 nM

